Biomedical Signal Processing and Control 69 (2021) 102925

Contents lists available at ScienceDirect

Biomedical Signal Processing and Control

journal homepage: www.elsevier.com/locate/bspc

Breast DCE-MRI segmentation for lesion detection by multi-level thresholding using student psychological based optimization

Dipak Kumar Patra [a,*], Tapas Si [b], Sukumar Mondal [c], Prakash Mukherjee [d]

[a] Research Centre of Natural and Applied Sciences (Department of Computer Science), Raja Narendralal Khan Women's College (Autonomous), Midnapore 721102, West Bengal, India
[b] Department of Computer Science and Engineering, Bankura Unnayani Institute of Engineering, Bankura 722146, West Bengal, India
[c] Department of Mathematics, Raja Narendralal Khan Women's College (Autonomous), Midnapore 721102, West Bengal, India
[d] Department of Mathematics, Hijli College, Kharagpur 721306, West Bengal, India

ARTICLE INFO

Keywords:
Breast cancer
Lesions
DCE-MRI
Segmentation
Entropy
Multi-level thresholding
Student Psychology Based Optimizer

ABSTRACT

In recent years, the high prevalence of breast cancer in women has risen dramatically. Therefore, segmentation of breast Dynamic Contrast-Enhanced Magnetic Resonance Imaging (DCE-MRI) is a necessary task to assist the radiologist inaccurate diagnosis and detection of breast cancer in breast DCE-MRI. For image segmentation, thresholding is a simple and effective method. In breast DCE-MRI analysis for lesion detection and segmentation, radiologists agree that optimization via multi-level thresholding technique is important to differentiate breast lesions from dynamic DCE-MRI. In this paper, multi-level thresholding using Student Psychology-Based Optimizer (SPBO) is proposed to segment the breast DCE-MR images for lesion detection. First, MR images are denoised using the anisotropic diffusion filter and then, Intensity Inhomogeneities (IIHs) are corrected in the preprocessing step. The preprocessed MR images are segmented using the SPBO algorithm. Finally, the lesions are extracted from the segmented images and localized in the original MR images. The proposed method is applied on 300 Sagittal T2-Weighted DCE-MRI slices of 50 patients, histologically proven, and analyzed. The proposed method is compared with algorithms such as Particle Swarm Optimizer (PSO), Dragonfly Optimization (DA), Slime Mould Optimization (SMA), Multi-Verse Optimization (MVO), Grasshopper Optimization Algorithm (GOA), Hidden Markov Random Field (HMRF), Improved Markov Random Field (IMRF), and Conventional Markov Random Field (CMRF) methods. The high accuracy level of 99.44%, sensitivity 96.84%, and Dice Similarity Coefficient (DSC) 93.41% are achieved using the proposed automatic segmentation method. Both quantitative and qualitative results demonstrate that the proposed method performs better than the eight compared methods.

1. Introduction

According to statistics from the World Health Organisation (WHO), breast cancer is first cancer to occur internationally. Around 200,000 women are affected by breast cancer in 2019–2020, according to the Indian Council of Medical Research (ICMR). The death rate is 55 percent. According to the 1,762,450 new cases of breast cancer are anticipated in 2019–2020 figures, and 606,880 deaths from cancer in the United States (American Cancer Society, 2019). The changing lifestyle of individuals in developed and developing countries raises the incidence of breast cancers among women mainly at ages 35–55, from conventional to modern. The incidence of breast cancers can be controlled by detecting breast cancers in their early phases [1]. In reducing the death rate, the need to detect breast masses and microcalcifications early and accurately play a very significant role. It is difficult to work with manual methods that radiologists fail to adopt because of the parallels between the presence of breast masses, microcalcifications, and the historical segmentation of such anomalies. The need for early detection calls for automated systems to be introduced to assist radiologists in the specific diagnosis of breast cancer, as well as for further follow-up of the treatments needed for patients. Screening procedures for breast cancer in MRI, self-examination, and clinical breast monitoring, ultrasound, and mammography [2]. For breast mass detection, mammography is an effective and reliable X-ray procedure. Digital mammography replaces film mammography, where patient breast images are obtained using special, high-quality computerized

* Corresponding author.
E-mail address: dpatra11@gmail.com (D.K. Patra).

https://doi.org/10.1016/j.bspc.2021.102925
Received 14 April 2021; Received in revised form 18 June 2021; Accepted 24 June 2021
Available online 7 July 2021

systems and are used for further studies, such as identification and evaluation. Microcalcifications and mass abnormalities that cause breast cancer are the most common. A mammogram made of high-intensity background, breast area, fat tissue, and breast masses, and microcalcifications is called the image produced by mammography. Mammary masses and microcalcifications occur in the epithelial and connective tissues of the breast region [3]. Radiologists can create errors that, due to fatigue, neglect important clues as the demand for mammogram processing increases [4]. Breast masses arise as a lump of various shapes and sizes in the breast region. Breast mass severity may be classified as benign and malignant. In a mammogram, microcalcifications are deposits of calcium that appear as small bright spots. Mammogram sensitivity depends on the density, age, and hormone levels of the patients, and 10–30% of breast cancers are not detected. The predictive value of this is less than 35% [5]. Therefore, other imaging modalities are required.

Breast DCE-MRI [6] is now widely used for breast cancer diagnosis. MRI is a major modality of image processing in medical diagnosis. In the interpretation (diagnosis) of breast cancers, the DCE-MRI has demonstrated extremely high sensitivity. In high-risk patients, MRI can identify cancers that are not evident in traditional imaging and can be added to the screen. Today, breast MRI is better than other types of imaging used to track the reaction to chemotherapy. Besides, its false-negative incidence is lower compared to other imaging modalities. Physicians are looking for ways to mitigate patient pain associated with biopsy (or another overtreatment) and health care providers are searching for ways to eliminate process-related excessive costs. Since detecting and measuring breast masses is difficult. To determine exactly where breast masses are located, researchers have developed several techniques. The evaluation of these techniques can be carried out based on how the techniques segment the true and false breast masses that can be defined by comparing the results obtained with the radiologist's ground truth markings [7].

As the benefits and challenges of early detection and classification of breast cancer are significant, introducing an integrated system to assist qualified radiologists would ensure that the process of interpretation is highly accurate. It is also widely used within medical image segmentation. But there are several disadvantages to this approach as well: the computational complexity and the results' sensitivity to the model parameters. A new breast DCE-MRI segmentation method based on multilevel thresholding using SPBO [8] has been introduced in this paper to overcome these difficulties. The SPBO algorithm is very fruitful when finding a good enough solution to the global optimum of a complex optimization problem. The benefit of the SPBO algorithm, such as a low number of parameters and a lack of local optimal trapping, is agreed to solve the problem of multi-level thresholding. The main goal of this paper is to use the SPBO algorithm to segment breast lesions in DCE-MRI so that better results are obtained with simple solutions and a complete search is achieved compared to the current methods. Shannon entropy maximization using SPBO is used in the current work to segment breast lesions in DCE-MRI. The performance of the proposed method is compared with PSO [9], DA [10], SMA [11], MVO [12], GOA [13], IMRF [14], HMRF [15], and CMRF [16] methods. The experimental results demonstrate that the proposed method performs better than the eight compared methods.

1.1. Contributions of this paper

The contribution of this paper may be outlined as follows:

1. An SPBO-based segmentation method is developed to segment the lesions in breast DCE-MRI.
2. The proposed method is compared with PSO, DA, SMA, MVO, GOA, IMRF, HMRF, and CMRF. The proposed method performs better than the eight compared methods.

1.2. Organization of the paper

The remaining of the paper is organized as the following: Section 2 discusses the related works. Materials and methodology are described in Section 3. This section includes the proposed segmentation method using the SPBO algorithm. Section 4 includes results and discussion. Finally, a conclusion with future works is given in Section 5.

2. Related works

Several methods for lesion identification and its characterization in breast DCE-MRI have been established in the recent past. Among them, Artificial Intelligence (AI), Machine Learning (ML), and Soft Computing (SC) based techniques are more common. There are also related works discussed here.

The Watershed technique developed by Cui et al. [17] for lesion detection in DCE-MR images. Dissecting the lesion into 2-D slices that have the largest region of the lesion starts with this technique. The Gaussian Mixture Model (GMM) measures context markers or marginal lesions and severity. The adaptive region growing and edge-based deface mass segmentation area method is implemented by Kozegar et al. [18]. Mass segmentation is a challenging task in Automated Breast Ultrasound Systems (ABUS) imaging because speckle noise in ultrasound images degrades the image quality. Breast masses are very different in shape, size, texture, and implementing a robust method that is invariant to these changes is difficult. Going to a higher dimension makes the problem more complex since the segmentation algorithm should extract 3-D objects. For this reason, despeckling is used, followed by area-creation pre-segmentation and fine 3 Dimension-deformable model segmentation. In this, the adaptive region increasing algorithm is used to provide a rough approximation of the mass boundary and the circularity. Mass training-based GMM is used to determine the similarity threshold.

Feng et al. [19] developed a cluster of Fuzzy C-Means (FCM) for breast lesion segmentation. In this analysis, information from each pixel, such as the intensity of its neighbors, is implemented by an FCM method based on Hausdorff distance. Depending on the mutual data in the space between the pixel and its neighbors, the surrounding area for each pixel is constant and not adaptive. Clustering costs are calculated using Euclid and Hausdorff distances. The segmentation assessment is done by balancing the results with those of 3 ground truth images segmented using a manual specialist. As a technique for breast lesion segmentation, Boss et al. [20] given the FCM clustering algorithm. The fourteen Haralick characteristics are taken out from the mammogram image applying the Gray Level Co-occurrence Matrix (GLCM) for dissimilar angles. By applying Mean Square Error (MSE) and Root Means Square Error (RMSE) tests, the achievement of the FCM segmentation is measured. For a section of the mammographic image, Valdes-Santiago et al. [21] used FCM and decision trees. In this, followed by segmentation of a Region of Interest (ROI) with FCM, contrast decrease, compactness, area, false positives using the filter, and contrast adaptive histogram equalization, the first original image is preprocessed. A binary decision tree categorization is used to extract the function that provides segmented mass. It utilizes image resizing and filtering, which shows the importance of fuzzy sets in the anomaly's edge life recognition. For breast lesion detection and segmentation, the K-means using GMM and Convolution Neural Network (CNN) are developed by Shamy and Dheeba [22]. The first phase is the ROI sector. Then, ROI texture extraction and feature optimization algorithms are used. The third step is a classification of detected abnormality as benign or malignant using CNN.

Hoffmann et al. [23] developed an automated segmentation of breast MRI lesions focused on the morphological, kinetic, Spatiotemporal, and joint segmentation-motion compensation process. Both morphological and kinetic features are derived and used as possible indicators for non-standard lesion detection. They used a novel term called Zernike

velocity moments as a special descriptor to describe the simultaneous action of these lesions' Spatio-temporal behavior. To capture the transient upgrade, Zheng et al. [24] built up the spatiotemporal-improvement architecture highlights from a Discrete Fourier Transformation (DFT), trailed by a proportion of the second invariants of Hu and the Gabor surface highlights to capture the spatial varieties of each of the DFT coefficient maps. By using a direct classifier for twenty-two malignant and fifteen benign lesions, they showed a distinct under the Area Under the Receiver Operating Characteristic (ROC) Curve (AUC) of 0.97. To capture the spatiotemporal changes in breast lesions, Shannon et al. [25] developed the advantage of the gradient, first-order, and second-order (Haralick) textural features. The kinetic curve of each feature is defined by measuring its mean value at any point in time in all the lesions. To combine the parameters taken from the probabilistic boosting-tree classifier, an adequate model of textural-kinetic curves is used. Based on the 41 DCE-MRI breast studies, the kinetic and lesion morphology features of signal strength are outperformed by reported textural-kinetic features. Accuracy 90 percent and 0.92 AUC (95% sensitivity, 82% specificity) are given by the classifier. Using the multichannel Gabor channel bank, Torrents-Barrena et al. [26] calculated the highlights of the tissue from the ideal regions and applied the multi estimation preparation windows in the tumor territory to measure the highlights. A Quadratic Discriminant Analysis (QDA) applied by Honda et al. [27] on features taken out from DCE-MR image of breast masses, namely dynamic commutes in signal strength, abnormal of form, and margin smoothness. The system reached 85.6% accuracy, 87.1% sensitivity, and 82.1% specificity of classification. Lee et al. [28] established spatiotemporal enhancement patterns to allow for the distinct diagnosis of DCE-MRI breast lesions. The method used a 3-pronged approach to understand the various elements of the spatio-temporal lesion-enhancement pattern relationship: characteristic kinetic pixel-wise plotting, take out of spatial relationship characteristics from the spatial feature level, pixel-wise kinetic characteristic maps, and take out the function of kinetic relation. They announced an AUC of 0.88 using a Least-Squares Support Vector Machine (LSSVM) with configured second-and third-order function subgroups. To be stable and generalizable in various protocols, their Computer-Aided Diagnosis (CAD) approach may have lost some efficacy.

The feature extraction method based on curvelet transformation suggested by Francis et al. [29] to determine the anomalies in breast thermograms and they extracted the tissue features according to the curvelet region from the breast thermogram. Gupta and Tiwari [30] segmented image and binary erosion using the Otsu method. In the image, the histogram is updated for better understanding, classification, and visual study using the histogram softening feature, gray relational scanning for optimization, and histogram equalization. After normalization is performed to render the mean brightness difference high. Segmentation is finally performed using the method of Otsu thresholding, obeyed by a binary decrease for the foreground pixel area reducing maximum. It overcomes the problem of using local contrast enhancement methods to concentrate on methods of edge perception and upgrades the mammogram images' global and local contrast. A pixel-driven approach based on the thresholding of an Otsu and morphological refinements after processing suggested by Vignati et al. [31]. The acquired breast mask is still over-segmented, but there is always secret whole breast parenchyma. Arora et al. [32] developed a statistical recursive method via multilevel thresholding for segmentation of the image. It begins from the 2 utmost ends of the histogram and recursively applies the method until the segmented image does not dramatically change. Although this method is quite basic, it takes the histogram of the image as a Gaussian distribution and only uses the even number of thresholds.

Kom et al. [33] developed local adaptive thresholding to automated detection of masses in mammograms. To begin, the original image is enhanced using a method based on a linear transformation filter that modifies the local contrast of each pixel. Second, obtain an image with segmented masses by subtracting the augmented image from the original image. Binarization of the latter using a local adaptive thresholding approach is the final stage. The sensitivity of this proposed approach reached up to 95.91 percent when it tested on a series of 61 mammograms. Ribes et al. [34] proposed a Markov Random Field (MRF)-based statistical approach for the automatic segmentation of breast MR images. Due to the gradient value of the image, this technique is known as spatially anisotropic and offers a trade-off between sound reduction and better protection of the image's edges. Singh et al. [35] developed a Conditional Generative Adversarial Network (CGAN) to break mammographic masses from an ROI. The generator model has learned to present lesions to create binary masks. Although evolutionary networks have learned features that distinguish the real public from the binary masks produced, their proposed CGAN's primary advantage is that it can work well for small datasets. Their method's results indicate higher coefficient values and coefficient correlations than those of the expected populations with ground realities. The method also classifies identified populations into 4 types (e.g., using CNN irregular, lobular, oval, and round).

Multi-Stage Transfer Learning implemented by Samala et al. [36], using deep neural networks for Digital Breast Tomosynthesis (DBT). First, in a multi-stage shift process, the ImageNet information captured the mammogram image data and then configured it for DBT image data. Data secured for mammography and then DBT data. Subsequently, the structure of most CNN separates the first layer of refrigeration convection with two transmission networks. The method of neural networks manages the learning algorithm well with accuracy. Saha and Chakraborty [37] developed for the identification and segmentation of membranes and nuclei in breast tumor estimation using Her2Net. Images of colored cytoplasm with Her2Net monoclonal antibodies are the most important phenomenon. In the case of research and training data sets, data cohort performance is closely related to output metrics, in which case data can be used. The proposed rate Her2Net indicates a very low False-Positive Rate (FPR).

Agner et al. [38] developed an automatic segmentation of triple-negative breast cancers. Triple negative (TN) breast cancer is a molecular subtype in which the estrogen, progesterone, and HER2 receptors are not expressed. Targeted treatments are unsuccessful due to a lack of receptor expression, so chemotherapy is currently the only option. They tested a CAD system's ability to quantitatively differentiate triple-negative breast cancers from other molecular subtypes of breast cancer on DCE-MRI, as well as to distinguish benign from malignant lesions on DCE-MRI. They applied an Expectation–Maximization (EM) driven active scheme for the segmentation of breast lesions in DCE-MRI. The morphological, textural, and kinetic characteristics are then taken out and categorized by employing the Support Vector Machine (SVM). The system achieved 83% accuracy, 79% sensitivity, and 88% specificity.

Aghaei et al. [39] developed a computer-aided identification system to separate breast areas and tumors on breast MR images and computed a total of 39 kinetic image characteristics from both tumor and background parenchymal enhancement regions. The authors next used two ways to differentiate between complete response and nonresponse situations, which they tested. The first looked at each feature and combined the classification results from numerous features using a basic feature fusion algorithm. The second method used a leave-one-case-out validation method to optimize an attribute chosen classifier that combines an Artificial Neural Network (ANN) with a wrapper subset evaluator.

Reddi et al. [40] developed a criterion function that is obtained by concluding that an image's gray level histogram is a continual probability function. Even though these techniques bring down the cost of computing to some degree, completion time is stock-still a problem. The breast model developed by Tuncay and Akduman [41] using the realistic microwave through T1-weighted 3-D MRI data. For functional numerical three-dimensional microwave breast styles, this technique is used to create discrete shapes, sizes, and tissue compactness. Retter et al. [42]

applied a CAD scheme to identify non-mass gain and concentrated tumors. Motion recompense has been achieved through an optical flow mechanism. Subsequently, the lesions of the region-growing method used in the section. As a new component, different dynamic and morphological characteristics, like the Minkowski function, are extracted from split lesions with radial Krawchuk moments. Visual assessment of morphologic properties is a highly inter-observer variable, while automated computation of features leads to more reproducible indices and thus to a more standardized and objective diagnosis. In this context, experts explore innovative mathematical descriptors for both morphology and dynamics and also compare their effectiveness related tiny lesion classification based on innovative feature selection techniques.

In this paper, the entropy maximization-based segmentation of breast DCE-MRI using the metaheuristics algorithm SPBO is proposed. In the next section, the proposed method is described.

3. Materials & methodology

3.1. DCE-MRI dataset

Total 300 Sagittal T2-Weighted DCE-MRI 2D slices of 50 patients have been taken from Cancer Genome Atlas Breast Invasive Carcinoma (TCGA-BRCA) [43,44]. All MRI slices having a size greater than 256 × 256 are resized to 256 × 256. The ground truths are generated by manual segmentation by the expert radiologist and it is considered as the gold standard [45]. In the ground truth images, the pixels that belong to the lesions are assigned the true value and all other pixels are assigned false.

3.2. Proposed method

In this paper, a new breast DCE-MRI segmentation method for lesion detection is developed using SPBO. SPBO algorithm is a recently developed metaheuristic algorithm that has shown its better-searching ability than its competitive algorithms for solving benchmark function optimization problems. SPBO algorithm is never used before in image segmentation as well as in breast DCE-MRI segmentation. On the other hand, till multi-level thresholding technique is not used in breast DCE-MRI segmentation for lesion detection. Therefore, the SPBO algorithm is applied in the multi-level thresholding technique to search suitable threshold values through entropy maximization for breast DCE-MRI segmentation. The proposed method has three steps as the following:

1. Preprocessing
2. Segmentation
3. Postprocessing

The outline of the proposed SPBO-based segmentation method is given in Fig. 1.

3.3. Preprocessing

Both the clinical diagnostic functions and the segmentation process are affected by the noise in MRI [46]. The segmentation process also faces difficulties because of the presence of IIHs in MR images. IIHs are the smooth intensity change inside the originally homogeneous region in the MRI [14]. In this work, the MR images are denoised using Anisotropic Diffusion Filter (ADF) [46], and IIHs are corrected using Max filter-based method [47]. In MR images, noise is observed independent of inhomogeneity. The inhomogeneous image ($\mathscr{I}_h$) is modeled as defined by:

$$\mathscr{I}_h = \mathscr{I} \times \mathscr{B} + \mathscr{N} \tag{1}$$

where $\mathscr{I}$ is the homogeneous image, $\mathscr{B}$ is inhomogeneity bias field and $\mathscr{N}$ is noise. Denoising using ADF is discussed in the subsection.

3.3.1. Denoising using Anisotropic Diffusion Filter

An ADF is a technique that focuses on removing image noise without changing notable segments of the content of the image. In [48], ADF bears a resemblance to an action that generates a scale area, where an image based on a diffusion process creates a parameterized family of successively more obscure images. Each image obtained as a result of this process is stated as a transition between the image and a 2-D isotropic Gaussian filter, the widths of the filters increase with the parameters. This evolutionary action is a linear and spatial transmutation of the initial image. ADF is a generalization of this isolated action: it generates a family of parameterized images, but every result image turns on the localized content of the initial image, which is a combination of the initial image and filter image.

Let $\Omega \subset \mathbb{R}^2$ indicates a subset of the plane and a family of gray scale image indicates $I(.,t) : \Omega \rightarrow \mathbb{R}$, then ADF is designated as follows

$$\frac{\partial I}{\partial t} = div\,(c(u,v,t)\nabla I) = \nabla c.\nabla I + c(u,v,t)\triangle I \tag{2}$$

where $\triangle$ indicates the Laplacian, the slope indicated by ∇, the divergence operator indicated by *div* and $c(u,v,t)$ indicates the diffusion

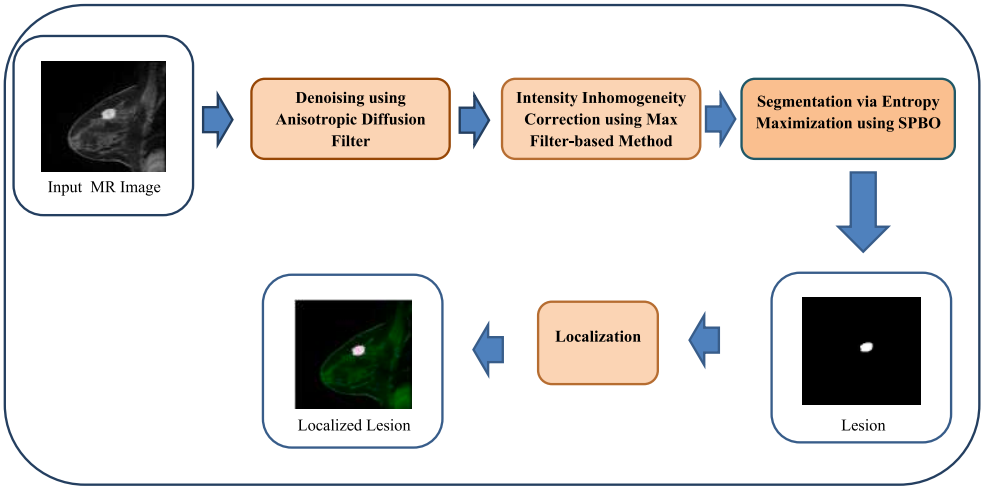

Fig. 1. Outline of the proposed method.

coefficient. The rate of diffusion denotes $c(u, v, t), (u, v)$ denotes spatial position, and t is the time parameter of process ordering. This is usually taken as a task of the image slope so that the edges of the image can be saved.

3.3.2. Max filter-based Intensity Inhomogeneity correction

After denoising, the image model in Eq. (1) is become as follows:

$$\mathscr{I}_h = \mathscr{I} \times \mathscr{B} \tag{3}$$

The steps of max filter-based Intensity Inhomogeneity (IIH) correction method [4] are as follows:

1. The max filter is applied to inhomogeneous image ($\mathscr{I}_h$) and the result is considered as the filtered image ($\mathscr{I}_b$):

$$\mathscr{I}_b = Max(\mathscr{I}_h) \tag{4}$$

2. Log of the filtered image ($\log(\mathscr{I}_b)$) is subtracted from that of the inhomogeneous image ($\log(\mathscr{I}_h)$) and result is considered as corrected image ($log(\mathscr{I}_c)$):

$$log(\mathscr{I}_c) = \log(\mathscr{I}_h) - \log(\mathscr{I}_b) \tag{5}$$

3. The corrected image ($\mathscr{I}_c$) is achieved as follows:

$$\mathscr{I}_c = \exp(log(\mathscr{I}_c)) \tag{6}$$

4. Intensity is adjusted to preserve initial dynamics as follows:

$$\mathscr{I}_{norm} = \frac{\mathscr{I}_c - \min(\mathscr{I}_c)}{\max(\mathscr{I}_c) - \min(\mathscr{I}_c)} \times \max(\mathscr{I}_h) \tag{7}$$

where $\mathscr{I}_{norm}$ is the normalized image.

3.4. Segmentation

Segmentation is the method of separating lesions by breaking DCE-MRI into non-overlapping sections from the background portions. This segmentation method of searching the breast lesions is carried out by several algorithms, such as classical methods, global thresholding, and local thresholding based on image histograms. This paper proposes area growth that comes under pixel-based techniques where thresholds for seed points and homogeneity criteria are created using the SPBO method, which is a metaheuristic optimization algorithm.

3.4.1. Entropy maximization

After the de-noised image is collected, entropy maximization is performed to determine segmentation threshold values. The explanation for maximizing entropy is to maximize the various number of homogeneous locations between. The image histogram is determined to make the pixel frequency available in the image. Then pixel frequencies from histograms are used to measure the entropy value. Here entropy function H is the objective function to be maximized by applying the algorithm SPBO. The expected solutions here are integer values in the range [0, 255] since the image has gray values from 0 to 255.

Shannon's entropy theory [49] is a key theory in the domain "information theory and coding". This theory is used to probabilistically determine the amount of information transmitted by any data. Let us assume that an image has $(k+1)$ homogeneous areas and k threshold gray levels at $t_1, t_2, t_3, \cdots, t_k$.

$$h(i) = \frac{f_i}{N} \qquad i = 0, 1, 2, \cdots, 255.$$

where f_i denotes the frequency of i^{th} gray level, N denotes the total number of gray levels present in the image, and $h(i)$ denotes normalized frequency.

Shannon Entropy function is outlined as

$$H = -\sum_{i=0}^{t_1} P_{1i}\ln(P_{1i}) - \sum_{i=t_1+1}^{t_2} P_{2i}\ln(P_{2i}) - \cdots - \sum_{i=t_k}^{255} P_{ki}\ln(P_{ki}) \tag{8}$$

where,

$$P_{1i} = \frac{h(i)}{\sum_{i=0}^{t_1} h(i)} \qquad \text{for } 0 \leqslant i \leqslant t_1,$$

$$P_{2i} = \frac{h(i)}{\sum_{i=t_1+1}^{t_2} h(i)} \qquad \text{for } t_1 + 1 \leqslant i \leqslant t_2,$$

$$P_{ki} = \frac{h(i)}{\sum_{i=t_k+1}^{255} h(i)} \qquad \text{for } t_k + 1 \leqslant i \leqslant 255.$$

Shannon entropy function H in Eq. (8) is applied as an objective function to be maximized using SPBO for getting optimum threshold values.

3.4.2. Student psychology based optimization

In [8], the authors defined and studied a Student psychology-based optimization algorithm for solving student overall performance in the classroom based on the student's psychology. Throughout this study, authors characterized students by four categories i.e., best student, good student, average student, and students who try to improve randomly.

Best student: The student who has the most elevated generally test marks/grades are supposed to be the best student in the class. Psychological tendency of best student will consistently try to hold her/his place. It is possible to convey the progress of the best student with the help of Eq. (9).

$$X_{bestnew} = X_{best} + (-1)^k \times rand \times (X_{best} - X_j) \tag{9}$$

where, respectively, X_{best} and X_j are the marks obtained by the best student in a given subject and a randomly selected j^{th} student. *rand* is a random number in span 0 and 1, and the parameter k is selected as either 1 or 2. $X_{bestnew}$ denotes the progress of the best student. The best student's primary aim is to maximize her/his performance in each subject to increase her/ his overall marks and to retain her/his best place.

Good student: If a student is interested in some subject, then he or she will try to enhance his or her overall performance more and more. Because different student psychologies are different, the selection of this student category is a random activity. This category of the student may be represented with the help of Eq. (10). At the same time, certain students try to make more effort in their studies than the average student's efforts. As well as trying to pursue the effort offered by the best student. With the assistance of Eq. (11), this type of student can be expressed.

$$X_{newi} = X_{best} + [rand \times (X_{best} - X_i)] \tag{10}$$

$$X_{newi} = X_i + [rand \times (X_{best} - X_i)] + [rand \times (X_i - X_{mean})] \tag{11}$$

where, X_i is the i^{th} student's marks/grade obtained in that subject, X_{mean} is the class's average output in that specific subject.

Average student: The students will attempt to invest more energy into different points to improve their general scores, despite the fact that they put forth a normal attempt towards this subject. As the normal subject-savvy understudy, this class of students can be recognized. Performance of this category of the student may be represented by using Eq. (12)

$$X_{newi} = X_i + [rand \times (X_{mean} - X_i)] \tag{12}$$

where, X_i and X_{mean} are, in order, the marks achieved by the i^{th} particular

subject.

Students who try to improve randomly: A few students expect to improve their presentation all alone, except for those three gatherings of students referenced previously. Somewhat, they attempt to haphazardly offer exertion to the point, contingent upon the subject. This sort of student attempts to arbitrarily offer exertion to the subject with the goal that the general presentation increments in the investigation. Performance of this category of the student may be represented with the use of Eq. (13)

$$X_{newi} = X_{min} + [rand \times (X_{max} - X_{min})] \tag{13}$$

where X_{min} is the minimum marks of the subject and X_{max} is the maximum of marks of the subject.

Algorithm 1 presents the pseudo-code of this algorithm.

Algorithm 1. SPBO

```
Initialize the population and converging criteria
Evaluate the initial performance of the class
while P <= Maximum iteration do
  for m = 1 to number of subject offered do
    for each student check the category of the student do
      if the student is the best student then
        Modify performance using Eq. (9)
      end if
      if the student is a good student then
        for each student check whether the student is following the best student only do
          if Yes then
            Modify performance using Eq. (10)
          else
            Modify performance using Eq. (11)
          end if
        end for
      end if
      if the student is the average student then
        Modify performance using Eq. (12)
      else
        Modify performance using Eq. (13)
      end if
    end for
    Check the boundary
    Evaluate the performance of the class
    if the new performance is better then
      Replace the old performance with the new one
    else
      Keep the old performance
    end if
    m = m + 1
  end for
  P = P + 1
end while
Display the performance of the best optimum solution
```

3.5. Postprocessing

After obtaining the segmented image from the segmentation process of DCE-MRI, the lesions are extracted. In DCE-MRI, the pixels belong to the regions of lesions having hyper-intensities. Therefore, the segment labels of the regions of lesions having the highest values, and segment images are thresholded using the highest segment labels. Lesions are extracted from the original MR images using the thresholded binary images and localized in the original MR images.

4. Results & discussion

In this paper, the lesion segmentation method for breast DCE-MRI is proposed. The MR images contain noise and IIHs due to which the segmentation process faces difficulties. Therefore, the noise is removed from MR images using an anisotropic diffusion filter, and IIHs are corrected in the preprocessing step. The parameters of compared algorithms are adopted from their original papers. The parameter settings are given in Table 1. The PC configuration is given in Table 2.

Table 1
The parameter settings of algorithms.

Algorithm	Parameter	Value
SPBO	Number of search agents	30
	Maximum number of iterations	100
PSO	Swarm size (N)	30
	Inertia weight (W)	0.72984
	Personal cognizance (C_1)	1.49618
	Social cognizance (C_2)	1.49618
	Maximum number of iterations	100
DA	Number of search agents	30
	Maximum number of generations	100
SMA	Number of search agents	30
	Maximum number of iterations	100
MVO	Number of search agents	30
	$WEP_{\max}$	1
	$WEP_{\min}$	0.2
	Maximum number of iterations	100
GOA	Number of search agents	30
	cMax	1
	cMin	0.00004
	Maximum number of iterations	100
IMRF	Maximum number of iterations	100
HMRF	EM iterations	5
	MAP iterations	5
CMRF	Potential	0.5
	Maximum number of iterations	100

Table 2
PC configuration.

Name	Configuration
CPU	Intel® Core™ i3-8130U @ 2.20 GHz.
RAM	4 GB
Operating System	Windows 7 Ultimate (64-bit)
Software	MATLAB 2017b

The performance assessment parameters [50,51] for SPBO are estimated based on the method of breast lesion segmentation. Parameters are used such as Accuracy, Sensitivity, Specificity, Precision, FPR, F-measure, Geometric Mean (G-mean), and DSC. Let TP be the True Positive rate, FP be the False Positive rate, TN be the True Negative rate, and FN be the False Negative rate. The different performance measures are defined as follows:

$$Accuracy = (TP + TN)/(TP + FN + TN + FP) \tag{14}$$

$$Sensitivity(recall) = TP/(TP + FN) \tag{15}$$

$$Specificity = TN/(TN + FP) \tag{16}$$

$$Precision = TP/(TP + FP) \tag{17}$$

$$FPR = 1 - Specificity \tag{18}$$

$$F - measure = \frac{2 \times recall \times precision}{recall + precision} \tag{19}$$

$$G - mean = \sqrt{Sensitivity \times Specificity} \tag{20}$$

DSC is used to evaluate the performance quantitatively. DSC is calculated as follows:

$$DSC(A, B) = \frac{2|A \cap B|}{|A| \cup |B|} \tag{21}$$

where A and B are binary masks for the segmented lesion and ground truth, respectively. The overlapping ratio of the observed lesion to the ground truth in the MRI is indicated by DSC. The higher DSC values indicate improved performance.

As the SPBO method starts with the randomly initialized population, the same experiments repeated 10 times for a single image. The quantitative results in terms of the mean and standard deviation of performance evaluation metrics over 10×300 results are considered for analysis. The proposed method is evaluated and analyzed, together with the existing PSO, DA, SMA, MVO, GOA, HMRF, IMRF, and CMRF methods.

4.1. Quantitative results

The quantitative results (i.e., performance evaluations) of the proposed method compared to other methods are illustrated in Table 3. The box plot (methods versus different performance measures) of comprehensive performance of different methods over 300 MR images is given in Figs. 2–9.

It is observed from the quantitative results in Table 3, the mean classification accuracy obtained from the proposed method is higher than that obtained from PSO, DA, SMA, MVO, GOA, HMRF, IMRF, and CMRF. The accuracy of SPBO is 99.44% which is higher than all methods. The mean sensitivity is 96.84% and the mean specificity is 99.56% obtained from the proposed method is also higher than those obtained from PSO, DA, SMA, MVO, GOA, HMRF, IMRF, and CMRF methods. Precision is another key measure of lesion detection. The mean precision value of SPBO is 93.87% whereas the mean precision values of PSO, DA, SMA, MVO, GOA, HMRF, IMRF, and CMRF are respectively 82.79%,77.83%,84.88%,87.72%,84.87%,80.21%,82.82%, and 76.18% which are very low.

The mean G-mean scores of the proposed method is 96.94% which is also higher than that of PSO, DA, SMA, MVO, GOA, HMRF, IMRF, and CMRF. A higher mean G-mean score specifies that the classifier will solve the high-class imbalance problem, where the number of lesions in the breast MR images is very small compared to the healthy tissues.

The F-measure is applied to measure the trade-off between sensitivity and precision. The mean F-measure is 93.15% which is much higher for the proposed method than for PSO, DA, SMA, MVO, GOA, HMRF, IMRF, and CMRF. The F-measure is the accuracy of the classification for lesion tissues detected in the breast. The higher value of this indicator suggests that the lesions in breast MRI can be identified with greater accuracy by the SPBO classification.

FPR is also known as the false alarm rate, and it determines the ratio of the wrongly labeled negative samples to the overall negative sample count. Therefore, the specificity complements it. FPR is not responsive to data distribution changes and therefore both metrics can be implemented with imbalanced data. The mean FPR of the proposed method (SPBO) is 0.44% which is much lower than PSO, DA, SMA, MVO, GOA, HMRF, IMRF, and CMRF. The lower value of this measure indicates that negative samples are minimum in images.

The mean DSC value of the proposed method is 93.41% which is also higher than that of the methods of PSO, DA, SMA, MVO, GOA, HMRF, IMRF, and CMRF. The higher DSC value demonstrates a greater overlap with the ground truths of the segmented lesions. It is observed that the proposed SPBO-based segmentation methodology outperforms the PSO, DA, SMA, MVO, GOA, HMRF, IMRF, and CMRF from the study of the above quantitative data.

Robustness is another essential aspect of the methods of segmentation for lesion detection. It is measured in terms of the standard deviation of performance measurements over many runs, and a lower standard deviation indicates greater robustness. The standard deviation results in Table 3 are small compared to eight existing methods, so the proposed segmentation technique is robust for breast MRI lesion detection.

A boxplot is a graph that provides a good indication of how the values are spread out in the details. But, compared to a histogram or density plot, boxplots can seem primitive. It is observed from Fig. 2 that the proposed SPBO has a higher median accuracy of classification than the other methods. Since accuracy outcomes are compacted, the minimum difference and the maximum value are very low. It is also found from Fig. 3 that SPBO has a higher median sensitivity score than other techniques. It is observed from Fig. 4 that the suggested SPBO has a higher median specificity of classification than the other methods. It is also observed from Fig. 5 that SPBO has a higher median precision score than other methods. SPBO has a higher median G-mean, F-measure, FPR, and DSC score than other methods and that can be observed from Figs. 6–9. From the above results, it can be determined that SPBO has superior performance compared to PSO, DA, SMA, MVO, GOA, HMRF, IMRF, and CMRF. Likewise, the proposed method based on SPBO obtains the best values in terms of accuracy, sensitivity, specificity, precision, G-mean, F-measure, FPR, and DSC. These outcomes reflect the better segmentation of breast DCE-MRI for lesion detection.

4.1.1. Statistical analysis using ANOVA followed by Tukey HSD

For validation of the segmentation performance, the DSC parameter

Table 3
Mean and standard deviation (in parenthesis) of performance measure values (in %) for proposed method SPBO, existing methods PSO, DA, SMA, MVO, GOA, HMRF, IMRF and CMRF.

Performance Matrix	SPBO	PSO	DA	SMA	MVO	GOA	HMRF	IMRF	CMRF
Accuracy	**99.44** (0.0248)	99.02 (0.0260)	98.31 (0.0411)	98.76 (0.0387)	98.37 (0.0489)	98.10 (0.0376)	98.46 (0.0301)	98.83 (0.0310)	97.99 (0.0463)
Sensitivity	**96.84** (0.0552)	91.28 (0.1007)	89.58 (0.1357)	90.73 (0.1190)	89.93 (0.1171)	83.35 (0.1627)	90.51 (0.1373)	90.61 (0.1197)	89.89 (0.1501)
Specificity	**99.56** (0.0227)	99.09 (0.0259)	98.46 (0.0330)	98.88 (0.0353)	98.51 (0.0411)	98.29 (0.0494)	98.55 (0.0327)	98.99 (0.0433)	98.14 (0.0480)
Precision	**93.87** (0.0628)	82.79 (0.1752)	77.83 (0.1546)	84.88 (0.1159)	87.72 (0.1536)	84.87 (0.2250)	80.21 (0.1687)	82.82 (0.2521)	76.18 (0.2702)
G-mean	**96.94** (0.0620)	95.36 (0.0676)	94.44 (0.0503)	94.35 (0.0623)	94.15 (0.0686)	92.52 (0.0861)	95.99 (0.0607)	95.38 (0.0657)	95.79 (0.0684)
F-measure	**93.15** (0.0681)	84.99 (0.1027)	81.14 (0.0862)	85.62 (0.0691)	87.17 (0.1056)	88.23 (0.1440)	84.11 (0.1062)	83.07 (0.2118)	78.87 (0.2176)
FPR	**0.44** (0.0010)	0.91 (0.0106)	1.54 (0.0112)	1.12 (0.0051)	1.49 (0.0060)	1.71 (0.0048)	1.45 (0.0075)	1.01 (0.0037)	1.86 (0.0073)
DSC	**93.41** (0.0668)	84.99 (0.1027)	82.49 (0.0998)	85.14 (0.1112)	85.83 (0.0994)	81.06 (0.1779)	81.38 (0.1617)	83.07 (0.2118)	81.60 (0.1839)

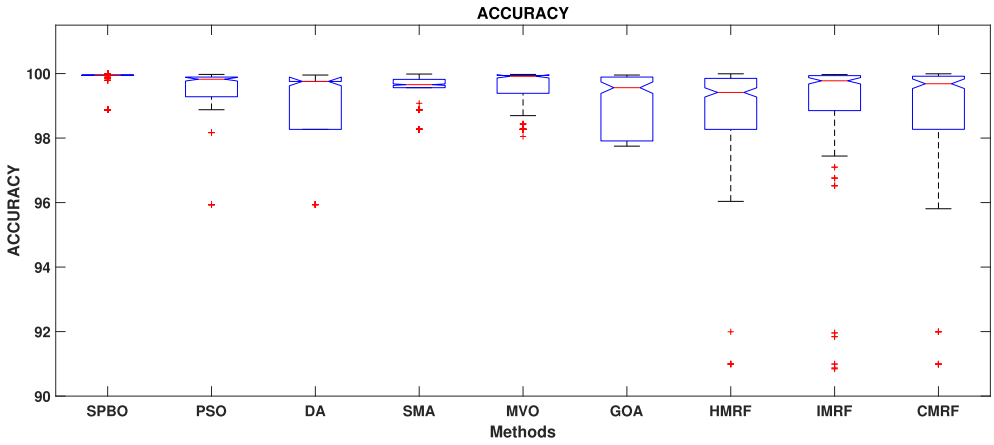

Fig. 2. The box plot (methods versus accuracy) of comprehensive classification performance of different methods over 300 MR Images.

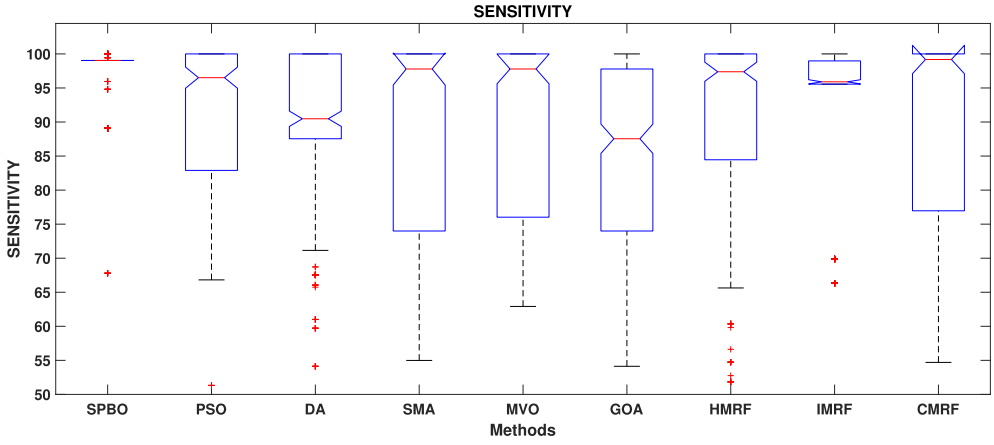

Fig. 3. The box plot (methods versus sensitivity) of comprehensive classification performance of different methods over 300 MR Images.

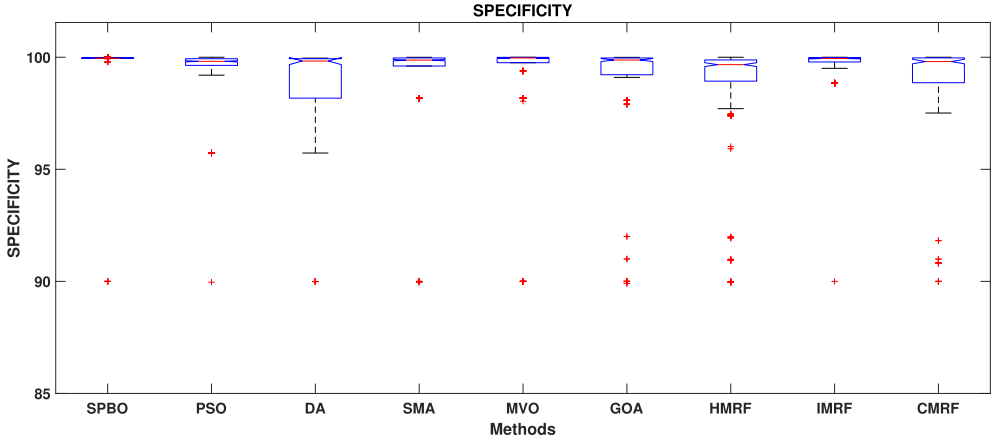

Fig. 4. The box plot (methods versus specificity) of comprehensive classification performance of different methods over 300 MR Images.

is used for statistical analysis using one-way ANOVA [52] followed by Tukey Honestly Significant Difference (HSD) [53]. The overlapping ratio of the segmented lesions to the ground truths in the MRI is indicated by DSC. The higher DSC values indicate better performance. The null hypothesis in the ANOVA test is:

H_0: all the methods are equivalent.
against the alternative hypothesis:
H_1: all the methods are not equivalent.

The ANOVA test result on the DSC is provided in Table 4. It is observed from Table 4 that the *p-value* of one way ANOVA test is $4.149E-32$ which is less than the significant level at $\alpha = 0.05$. Therefore, the performance of all the methods is not equivalent. After the ANOVA test, Tukey HSD statistical test is conducted for pair-wise comparison of the proposed SPBO-based method with the other methods and test results are provided in Table 5. From Table 5, it is observed that SPBO statistically outperforms other methods with a significance level $\alpha = 0.05$.

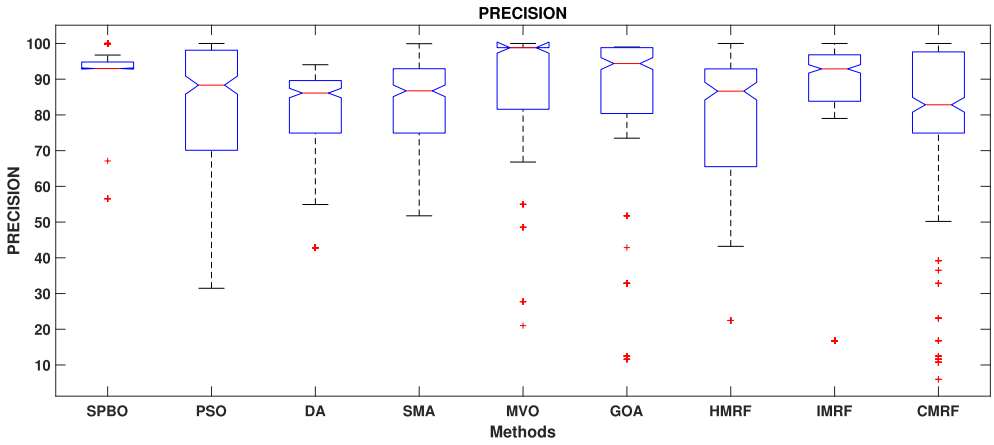

Fig. 5. The box plot (methods versus precision) of comprehensive classification performance of different methods over 300 MR Images.

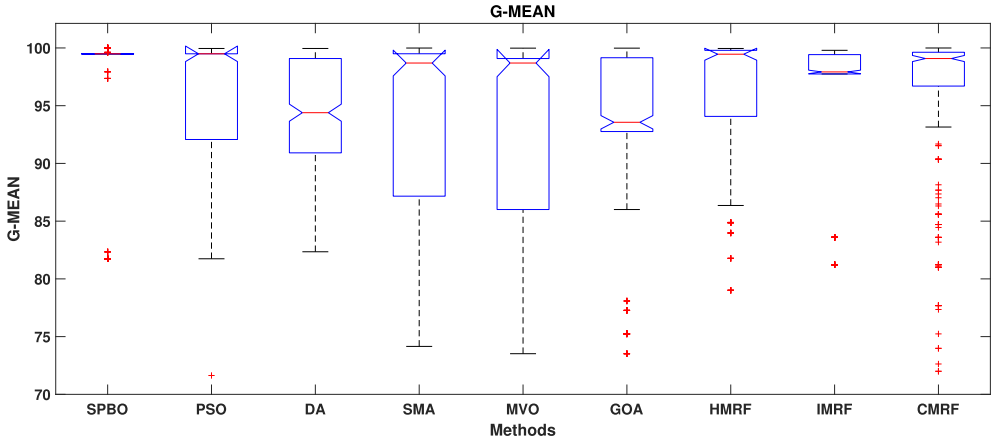

Fig. 6. The box plot (methods versus g-mean) of comprehensive classification performance of different methods over 300 MR Images.

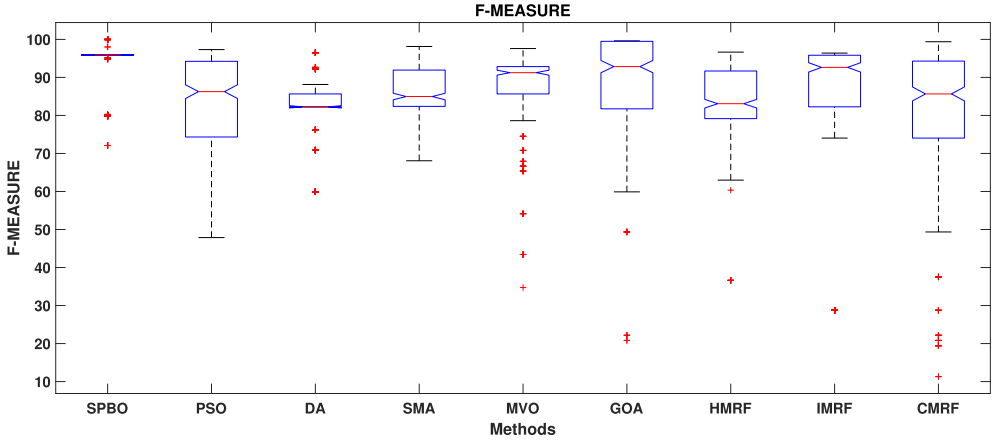

Fig. 7. The box plot (methods versus f-measure) of comprehensive classification performance of different methods over 300 MR Images.

4.1.2. Statistical analysis using Wilcoxon Signed Rank Test

A non-parametric test is conducted to analyze the performance of the algorithms. For a pair-wise comparison of the proposed SPBO algorithm with the other algorithms, the Wilcoxon Signed Rank Test [54] is performed. The statistical test results on the accuracy, sensitivity, specificity, precision, G-mean, F-measure, FPR, and DSC are described in Tables 6–13, respectively. Here, it is considered that the pair-wise null hypothesis is.

H0: The pair of methods are equivalent.
against the alternative hypothesis:
H1: The pair of methods are not equivalent.

The significant level of the test α is 0.01. The α value is adjusted using Bonferroni correction method [55]. The adjusted α value is $\widetilde{\alpha} = \alpha/\text{No. of comparison} = 0.01/8 = 0.00125$. It has been observed from Table 6, 7, 8 and 13 that SPBO statistically outperforms PSO, DA, SMA, MVO, GOA, HMRF, IMRF, and CMRF. Also from Tables 9,10 and 12, it has been

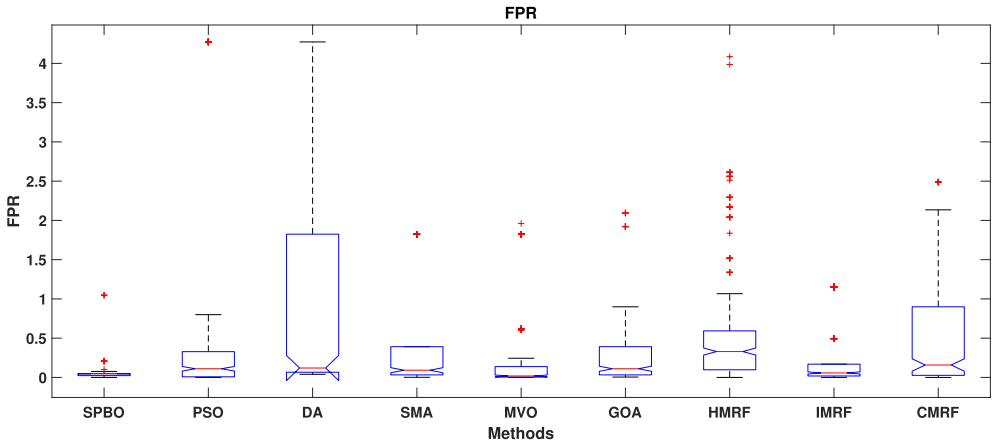

Fig. 8. The box plot (methods versus fpr) of comprehensive classification performance of different methods over 300 MR Images.

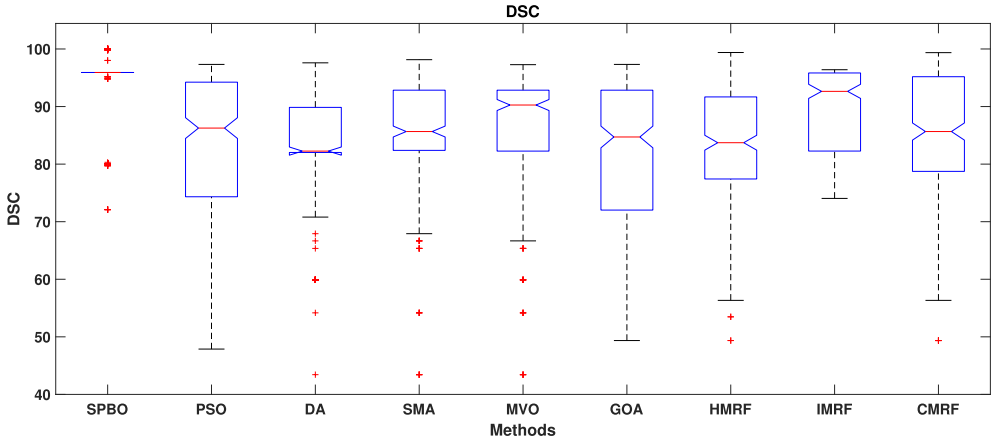

Fig. 9. The box plot (methods versus dsc) of comprehensive classification performance of different methods over 300 MR Images.

Table 4
ANOVA Test.

Source of Variance	SS	df	MS	F	*p-value*	F-crit.
Between Groups	35275.5697	8	4409.445497	21.58854223	4.149E−32	1.9418407
Within Groups	549634.9734	2691	204.2493398			
Total	584910.5373	2699				

Table 5
Tukey HSD Test Statistics based on DSC.

Sl. No.	Comparison	Comparison with T	Result
1	SPBO *vs* PSO	8.49 > 0.2089	Significant at $\alpha = 0.05$
2	SPBO *vs* DA	10.49 > 0.2089	Significant at $\alpha = 0.05$
3	SPBO *vs* SMA	8.27 > 0.2089	Significant at $\alpha = 0.05$
4	SPBO *vs* MVO	7.58 > 0.2089	Significant at $\alpha = 0.05$
5	SPBO *vs* GOA	12.35 > 0.2089	Significant at $\alpha = 0.05$
6	SPBO *vs* HMRF	12.03 > 0.2089	Significant at $\alpha = 0.05$
7	SPBO *vs* IMRF	10.34 > 0.2089	Significant at $\alpha = 0.05$
8	SPBO *vs* CMRF	11.81 > 0.2089	Significant at $\alpha = 0.05$

Table 6
Wilcoxon Signed Ranks Test Statistics on accuracy.

Sl. No.	Comparison	$p(2-tailed)$
1	SPBO *vs* PSO	0.0000001
2	SPBO *vs* DA	0.0000001
3	SPBO *vs* SMA	0.0000001
4	SPBO *vs* MVO	0.0000001
5	SPBO *vs* GOA	0.0000001
6	SPBO *vs* HMRF	0.0000001
7	SPBO *vs* IMRF	0.0000001
8	SPBO *vs* CMRF	0.0000001

observed that Precision, G-mean, F-measure, and FPR of SPBO are statistically higher significant than PSO, DA, SMA, IMRF, and CMRF. But there is no statistically significant difference in the Precision performance between SPBO and GOA. There is no statistically significant difference in the G-mean performance between SPBO and HMRF. There is no statistically significant difference in the G-mean performance between SPBO and GOA. There is also no statistically significant difference in the FPR performance between SPBO and MVO.

4.1.3. *Multi-Criteria Decision Analysis*

Multi-Criteria Decision Analysis (MCDA) [56] has become one of the

Table 7
Wilcoxon Signed Ranks Test Statistics on sensitivity.

Sl. No.	Comparison	$p(2-tailed)$
1	SPBO *vs* PSO	0.0000001
2	SPBO *vs* DA	0.0000001
3	SPBO *vs* SMA	0.0000001
4	SPBO *vs* MVO	0.0000001
5	SPBO *vs* GOA	0.0000001
6	SPBO *vs* HMRF	0.000003
7	SPBO *vs* IMRF	0.0000001
8	SPBO *vs* CMRF	0.001029

Table 8
Wilcoxon Signed Ranks Test Statistics on specificity.

Sl. No.	Comparison	$p(2-tailed)$
1	SPBO *vs* PSO	0.0000001
2	SPBO *vs* DA	0.0000001
3	SPBO *vs* SMA	0.000001
4	SPBO *vs* MVO	0.000549
5	SPBO *vs* GOA	0.0000001
6	SPBO *vs* HMRF	0.0000001
7	SPBO *vs* IMRF	0.0000001
8	SPBO *vs* CMRF	0.0000001

Table 9
Wilcoxon Signed Ranks Test Statistics on precision.

Sl. No.	Comparison	$p(2-tailed)$
1	SPBO *vs* PSO	0.0000001
2	SPBO *vs* DA	0.0000001
3	SPBO *vs* SMA	0.0000001
4	SPBO *vs* MVO	0.000055
5	SPBO *vs* GOA	0.003425
6	SPBO *vs* HMRF	0.0000001
7	SPBO *vs* IMRF	0.000003
8	SPBO *vs* CMRF	0.0000001

Table 10
Wilcoxon Signed Ranks Test Statistics on G-Mean.

Sl. No.	Comparison	$p(2-tailed)$
1	SPBO *vs* PSO	0.0000001
2	SPBO *vs* DA	0.0000001
3	SPBO *vs* SMA	0.0000001
4	SPBO *vs* MVO	0.0000001
5	SPBO *vs* GOA	0.0000001
6	SPBO *vs* HMRF	0.124219
7	SPBO *vs* IMRF	0.0000001
8	SPBO *vs* CMRF	0.000005

most significant and fastest-growing subfields of operations research/management science. MCDA means the process of evaluating the best feasible solution based on given requirements and issues that are common occurrences in daily life. Practical problems are also characterized by many non-commensurable and conflicting (competing) criteria, and all criteria may not be met simultaneously by any solution. In this work, the performance is analyzed using a well-known MCDA method namely Technique for Order of Preference by Similarity to Ideal Solution (TOPSIS). Here, multiple criteria are accuracy, sensitivity, specificity, precision, G-mean. F-measure, FPR, and DSC. FPR conflicts

Table 11
Wilcoxon Signed Ranks Test Statistics on F-Measure.

Sl. No.	Comparison	$p(2-tailed)$
1	SPBO *vs* PSO	0.0000001
2	SPBO *vs* DA	0.0000001
3	SPBO *vs* SMA	0.0000001
4	SPBO *vs* MVO	0.0000001
5	SPBO *vs* GOA	0.003534
6	SPBO *vs* HMRF	0.0000001
7	SPBO *vs* IMRF	0.0000001
8	SPBO *vs* CMRF	0.0000001

Table 12
Wilcoxon Signed Ranks Test Statistics on FPR.

Sl. No.	Comparison	$p(2-tailed)$
1	SPBO *vs* PSO	0.0000001
2	SPBO *vs* DA	0.0000001
3	SPBO *vs* SMA	0.0000001
4	SPBO *vs* MVO	0.024339
5	SPBO *vs* GOA	0.000018
6	SPBO *vs* HMRF	0.0000001
7	SPBO *vs* IMRF	0.000002
8	SPBO *vs* CMRF	0.0000001

Table 13
Wilcoxon Signed Ranks Test Statistics on DSC.

Sl. No.	Comparison	$p(2-tailed)$
1	SPBO *vs* PSO	0.0000001
2	SPBO *vs* DA	0.0000001
3	SPBO *vs* SMA	0.0000001
4	SPBO *vs* MVO	0.0000001
5	SPBO *vs* GOA	0.0000001
6	SPBO *vs* HMRF	0.0000001
7	SPBO *vs* IMRF	0.0000001
8	SPBO *vs* CMRF	0.0000001

with other criteria because low FPR values indicate better whereas higher values of other criteria indicate better. Table 14 described the MCDA ranked based on TOPSIS technique. From Table 14, it is observed that the SPBO method has the highest rank. After that PSO method follows the SPBO method. It is also observed that CMRF has the lowest rank.

4.2. Visual results

A total of 300 images of 50 patients have been used for the validation

Table 14
Multi-Criteria Decision Analysis rank based on TOPSIS technique

Methods	Rank
SPBO	1
PSO	2
IMRF	3
SMA	4
HMRF	5
MVO	6
DA	7
GOA	8
CMRF	9

of this method. Because of space limitations, 2 images of 2 different patients are displayed out of 300 test results. The segmented breast lesions using different methods are given in Fig. 10 for patient-1 and Fig. 11 for patient-2. The localized lesion images are given in Figs. 12 and 13 for patients 1 & 2 respectively.

From the qualitative results in Fig. 10 for patient-1, by comparing the SPBO segmented image in Fig. 10(c) with the ground truth image in Fig. 10(b), it can be easily observed that lesion regions are almost fully segmented by SPBO. The proposed SPBO-based method performs well in detecting lesions for the image. From the PSO segmented image in Fig. 10(d), it is observed that some lesions are not segmented by PSO. The PSO-based method does not perform well in the detection of lesions in the image as compared with the ground truth image. From DA segmented image in Fig. 10(e), it can be easily observed that some healthy tissues surrounding the lesion regions are detected as lesions by DA. This method does not perform well in the detection of the image as compared with the ground truth image. From SMA segmented image in Fig. 10(f), it is observed that SMA fails to segment the maximum of lesion regions in the image. From MVO and GOA segmented images in Fig. 10(g) and (h), it is observed that some lesions are not segmented by MVO and GOA. The two methods do not perform well in the detection of lesions in the image as compared with the ground truth image. From HMRF segmented image in Fig. 10(i), it is also observed that some healthy tissues are detected as lesions by HMRF like IMRF. This method also does not perform well in the detection of lesions in the image as compared with the ground truth image. From the CMRF segmented image in Fig. 10(k), it is observed that CMRF fails to segment the maximum of lesion regions in the image.

From the qualitative results in Fig. 11 for patient-2, by comparing the ground truth image in Fig. 11(b) and SPBO segmented image in Fig. 11 (c) for the MRI slice of patient-2, it can be easily observed that lesion regions are almost fully segmented by SPBO. The proposed SPBO-based method performs well in the detection of lesions in the image as compared with the ground truth image.

From Fig. 11(d) for MRI slice of patient-2, it can be easily observed that some healthy tissues are detected as lesions by PSO. The PSO-based method does not perform well in the detection of lesions in the image as compared with the ground truth image.

Fig. 11(e) and (f) depict that lesions are not segmented by DA and SMA at all. These methods become a failure in the detection of lesions in the image as compared with the ground truth image. From Fig. 11(g) for the MRI slice of patient-2, it can be easily observed that some healthy tissues are detected as lesions by MVO. The MVO-based method does not perform well in the detection of lesions in the image as compared with the ground truth image. From the CMRF segmented image in Fig. 11(h), it is observed that GOA fails to segment the maximum of lesion regions in the image. Fig. 11(i) and (j) depict that some healthy tissues are segmented by HMRF and IMRF. These methods do not perform well in the detection of lesions for the images as compared with the ground truth image.

Fig. 11(k) depicts that lesions are not segmented by CMRF at all. This method becomes a failure in the detection of lesions in the image as compared with the ground truth image.

Convergence graphs for the image patient-1 & 2 are given in Figs. 14 and 15 respectively. In the convergence graphs, the best objective function values i.e., entropy values against the function evaluations (FEs) are plotted. The convergence graph shows the progress of the search process towards the best solution. From the convergence graphs, it can be observed that the convergence behavior of SPBO is better than other metaheuristic algorithms. From the convergence graph in Fig. 14, it is observed that SPBO converges with a very close to the best result after about 500 FEs whereas PSO converges with a very close to its best result after about 1900 FEs. SPBO has a faster convergence rate than PSO after 300 FEs. SPBO has always better values than DA, MVO, SMA, and GOA. It is also observed that DA, MVO, SMA, and GOA are easily falling in the local optima (premature convergence). A similar observation can be made for the convergence graph in Fig. 15. Both convergence graphs show the better searching ability of the SPBO algorithm for entropy maximization.

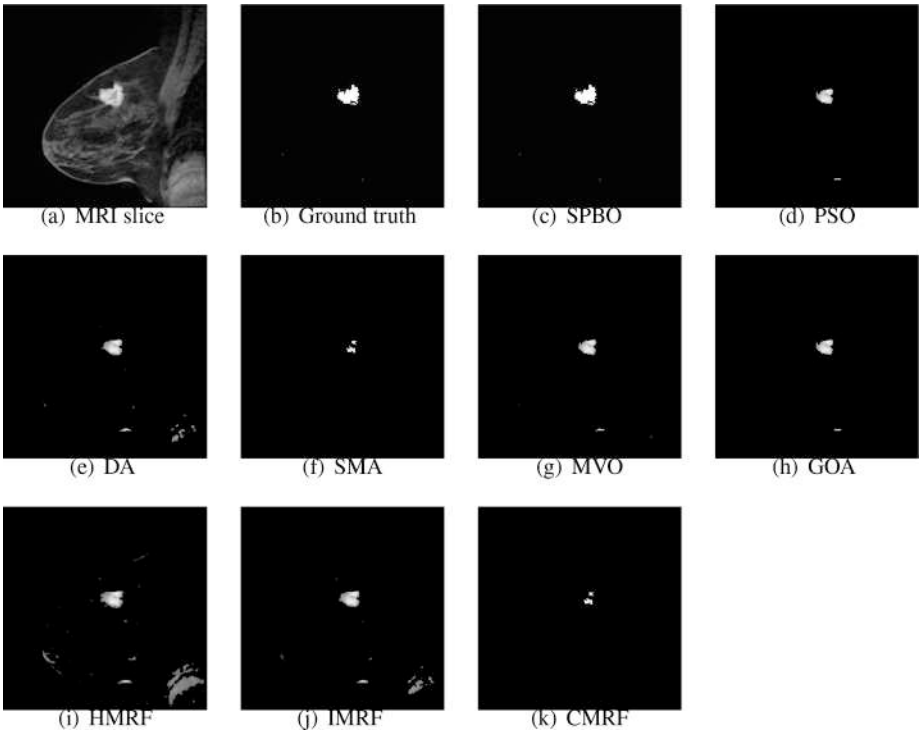

Fig. 10. For Patient-1 (a) Original MR image, (b) ground truth of MR image, (c) segmented image using SPBO, (d) segmented image using PSO, (e) segmented image using DA, (f) segmented image using SMA, (g) segmented image using MVO, (h) segmented image using GOA, (i) segmented image using HMRF, (j) segmented image using IMRF, and (k) segmented image using CMRF.

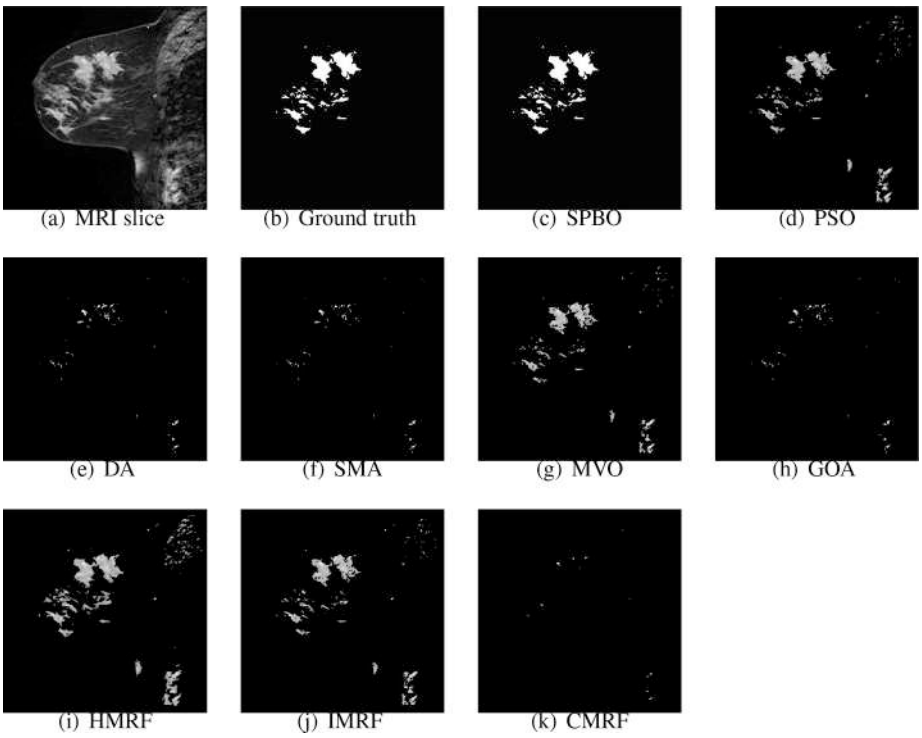

Fig. 11. For Patient-2 (a) Original MR image, (b) ground truth of MR image, (c) segmented image using SPBO, (d) segmented image using PSO, (e) segmented image using DA, (f) segmented image using SMA, (g) segmented image using MVO, (h) segmented image using GOA, (i) segmented image using HMRF, (j) segmented image using IMRF, and (k) segmented image using CMRF.

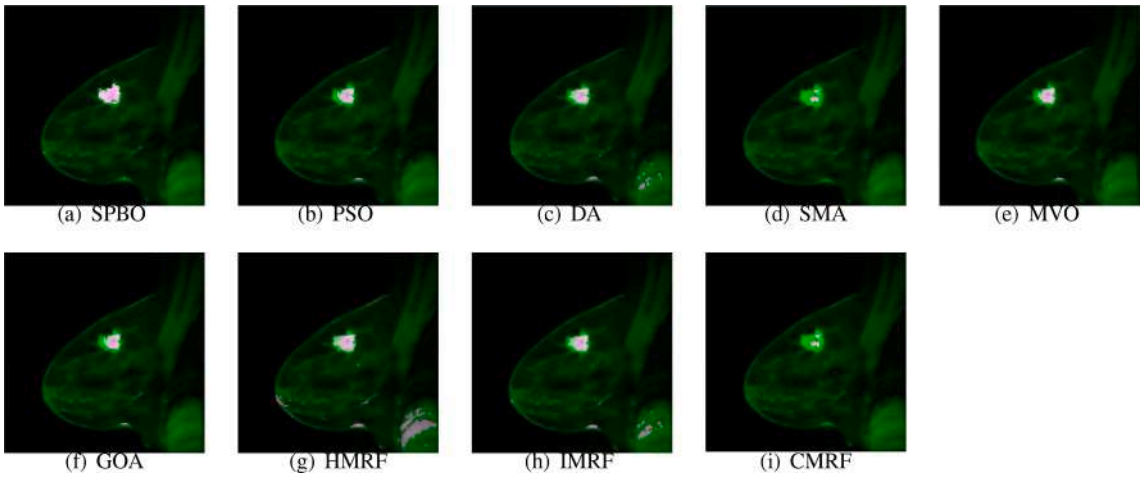

Fig. 12. Localized lesions (bright colored spot) in MR images for patient-1 (a) SPBO, (b) PSO, (c) DA, (d) SMA, (e) MVO, (f) GOA, (g) HMRF, (h) IMRF, and (i) CMRF.

4.3. Computational complexity

Table 15 shows the average CPU execution time for proposed and existing methods. The computational time for denoising and intensity inhomogeneities correction of each MR image is 0.26 s and 1.58 s, respectively.

From Table 15, it is observed that the average CPU execution time for SPBO is 2.4959 s. PSO takes an average execution time of 2.6114 s. DA takes an average execution time of 2.5809 s. SMA takes an average execution time of 2.6823 s. MVO takes an average execution time of 2.6153 s, GOA takes an average execution time of 2.6823 s, HMRF takes an average execution time of 2.6954 s, IMRF takes an average execution time of 2.7125 s and CMRF takes 2.8564 s. The SPBO is faster than all existing methods. From the above analysis of both quantitative and qualitative results, it is observed that SPBO performs better segmentation of breast lesion in DCE-MRI than PSO, DA, SMA, MVO, GOA, HMRF, IMRF, and CMRF. The experimental results demonstrate that SPBO is efficient and effective in lesion segmentation in breast DCE-MRI.

From the above discussion of quantitative and qualitative results, it may be concluded that the proposed method based on SPBO performs better than other compared methods in the segmentation of breast DCE-MRI for lesion detection. SPBO is efficient to find out the suitable threshold values for segmentation because SPBO has good searching ability and convergence characteristics.

5. Conclusion and future works

The goal of this study is to investigate and establish an effective

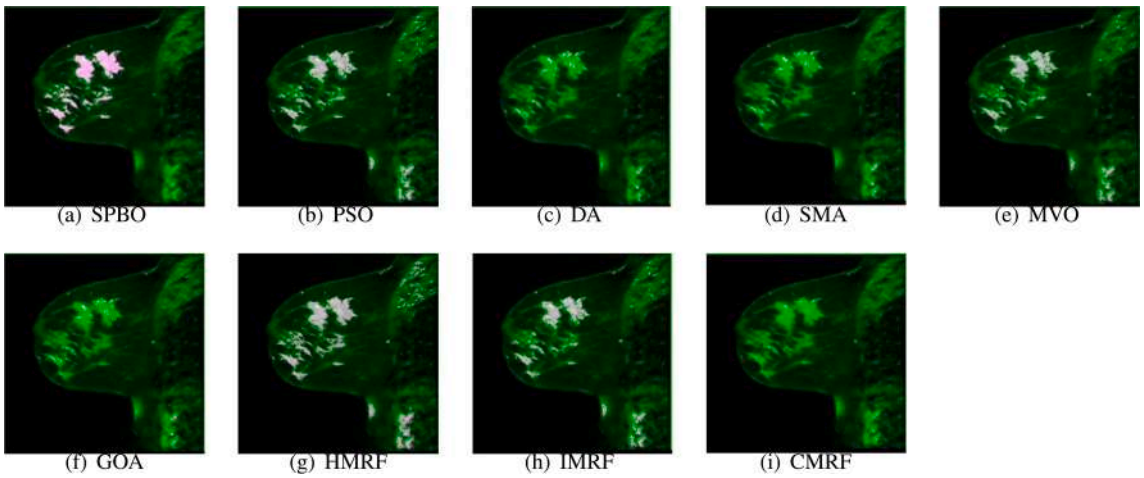

Fig. 13. Localized lesions (bright colored spot) in MR images for patient-2 (a) SPBO, (b) PSO, (c) DA, (d) SMA, (e) MVO, (f) GOA, (g) HMRF, (h) IMRF, and (i) CMRF.

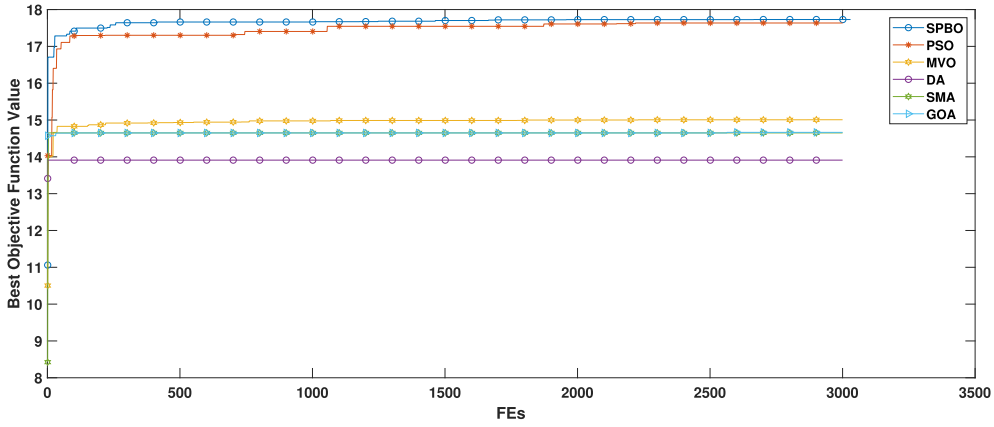

Fig. 14. Convergence graph for the DCE-MRI slice (Fig. 10(a)) of patient-1.

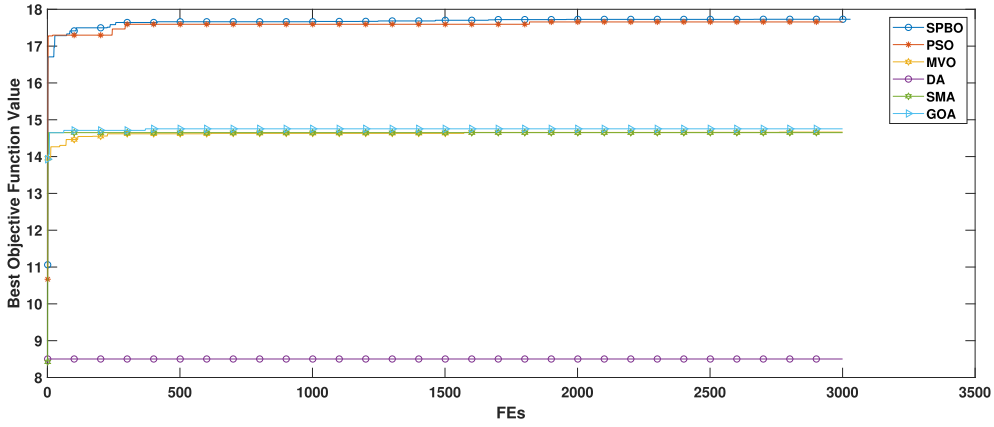

Fig. 15. Convergence graph for the DCE-MRI slice (Fig. 11(a)) of patient-2.

Table 15
The average CPU execution time for proposed method SPBO, existing methods PSO, DA, SMA, MVO, GOA, HMRF, IMRF, and CMRF.

Methods	SPBO	PSO	DA	SMA	MVO	GOA	HMRF	IMRF	CMRF
Execution time (seconds)	**2.4959**	2.6114	2.5809	2.6823	2.6153	2.6823	2.6954	2.7125	2.8564

method for breast DCE-MRI segmentation to assist the radiologist in diagnosis, treatment planning, and disease planning. SPBO-based method of segmentation is proposed in this paper. In this method, the SPBO algorithm is used to search for the optimal multilevel threshold values by maximizing entropy. Compared to the existing PSO, DA, SMA, MVO, GOA, HMRF, IMRF, and CMRF methods, the experimental results show the effectiveness of the proposed method that has achieved high performance in terms of accuracy, sensitivity, specificity, precision, F-measure, G-mean, and DSC. Compared with all existing methods, the experimental results indicate the efficiency of the proposed method. In the future, to dynamically evaluate the optimal number of thresholds, the Shannon entropy maximization using the SPBO algorithm will also be expanded. An improved version of the SPBO algorithm will be used to implement the MRI breast lesion segmentation method. The future works also include the development of breast MRI segmentation methods with feature selection techniques [57,58].

CRediT authorship contribution statement

Dipak Kumar Patra: Conceptualization of this study, Methodology, Software, Validation, Writing - review & editing. **Tapas Si:** Conceptualization of this study, Methodology, Supervision, Validation, Writing - original draft, Writing - review & editing. **Sukumar Mondal:** Conceptualization of this study, Writing - review & editing. **Prakash Mukherjee:** Conceptualization of this study, Writing - review & editing.

Declaration of Competing Interest

The authors declare that they have no known competing financial interests or personal relationships that could have appeared to influence the work reported in this paper.

References

[1] B. Verma, P. Zhang, A novel neural-genetic algorithm to find the most significant combination of features in digital mammograms, Applied Soft Computing 7 (2007) 612–625.

[2] J. Dheeba, S. Selvi, A swarm optimized neural network system for classification of microcalcification in mammograms, Journal of Medical System 36 (2012) 3051–3061.

[3] H.D. Cheng, X.J. Sh, R. Min, L. Hu, X.P. Cai, H.N. Du, Approaches for automated detection and classification of masses in mammograms, Pattern Recognition 39 (2006) 646–668.

[4] M. Pawar, S.N. Talbar, Genetic fuzzy system (GFS) based wavelet co-occurrence feature selection in mammogram classification for breast cancer diagnosis, Perspectives in Science (2016) 247–250.

[5] K.L. Kashyap, M.K. Bajpai, P. Khanna, Breast cancer detection in digital mammograms, in: IEEE International Conference on Imaging Systems and Techniques (IST), IEEE, 2015, pp. 1–6.

[6] R.M. Mann, C.K. Kuhl, K. Kinkel, C. Boetes, Breast MRI: guidelines from the european society of breast imaging, European Radiology 18 (2008) 1307–1318.

[7] W. Qian, F. Mao, X. Sun, Y. Zhang, D. Song, R.A. Clarke, An improved method of region grouping for microcalcification detection in digital mammograms, Computerized Medical Imaging and Graphics 26 (2002) 361–368.

[8] B. Das, V. Mukherjee, D. Das, Student psychology based optimization algorithm: A new population based optimization algorithm for solving optimization problems, Advances in Engineering Software 146 (2020).

[9] I.C. Trelea, The particle swarm optimization algorithm: convergence analysis and parameter selection, Information Processing Letters 85 (2002) 317–325.

[10] S. Mirjalili, Dragonfly algorithm: a new meta-heuristic optimization technique for solving single-objective, discrete, and multi-objective problems, Neural Computing & Applications 27 (2016) 1053–1073.

[11] S. Li, H. Chen, M. Wang, A.A. Heidari, S. Mirjalili, Slime mould algorithm: A new method for stochastic optimization, Future Generation Computer Systems 111 (2020) 300–323.

[12] S. Mirjalili, S.M. Mirjalili, A. Hatamlou, Multi-verse optimizer: a nature-inspired algorithm for global optimization, The Natural Computing Applications Forum 27 (2016) 495–513.

[13] S.Z. Mirjalili, S. Mirjalili, S. Saremi, H. Faris, I. Aljarah, Grasshopper optimization algorithm for multi-objective optimization problems, Applied Intelligence 48 (2018) 805–820.

[14] H. Zhang, S.W. Foo, S.M. Krishnan, C., Hua Thng, Computer aided detection of breast masses from digitized mammograms, in: IEEE International Workshop on Biomedical Circuits and Systems, IEEE, 2004, pp. 1–4.

[15] S.P. Chatzis, G. Tsechpenakis, The infinite hidden markov random field model, IEEE Transactions on Neural Networks 21 (2010) 1004–1014.

[16] G.R. Cross, A.K. Jain, Markov random field texture models, IEEE Transactions on Pattern Analysis and Machine Intelligence 5 (1983) 25–39.

[17] Y. Cui, Y. Tan, B. Zhao, L. Liberman, R. Parbhu, J. Kaplan, M. Theodoulou, C. Hudis, L. Schwartz, Malignant lesion segmentation in contrast-enhanced breast MR images based on the marker-controlled watershed, Medical Physics 36 (2009) 4359–69.

[18] E. Kozegar, M. Soryani, H. Behnam, T. Tan, Mass segmentation in automated 3-D breast ultrasound using adaptive region growing and supervised edge-based deformable model, IEEE Transactions on Medical Imaging 37 (2018) 918–928.

[19] Y. Feng, F. Dong, X. Xia, C.H. Hu, Q. Fan, Y. Hu, S. Mutic, An adaptive fuzzy c-means method utilizing neighboring information for breast tumor segmentation in ultrasound images, Medical Physics 44 (2017) 3752–3760.

[20] R. Boss, K. Thangavel, D. Daniel, Mammogram image segmentation using fuzzy clustering, in: International Conference on Pattern Recognition, Informatics and Medical Engineering (PRIME-2012), 2012, pp. 290–95.

[21] D. Valdes-Santiago, R. Quintana-Martinez, A. Leon-Mecias, M.L.B. Diaz-Romanach, Mammographic mass segmentation using fuzzy c–means and decision trees, in: International Conference on Articulated Motion and Deformable Objects, vol. 10945, 2018, pp. 1–10.

[22] S. Shamy, J. Dheeba, A research on detection and classification of breast cancer using k- means gmm & cnn algorithms, International Journal of Engineering and Advanced Technology 11 (2019) 315–320.

[23] S. Hoffmann, J.D. Shutler, M. Lobbes, B. Burgeth, A. Meyer-Bäse, Automated analysis of non-mass-enhancing lesions in breast mri based on morphological, kinetic, and spatio-temporal moments and joint segmentation-motion compensation technique, EURASIP Journal on Advances in Signal Processing 2013 (2013) 172.

[24] Y. Zheng, S. Englander, M. Schnall, D. Shen, Step: spatiotemporal enhancement pattern for MR-based breast tumor diagnosis, Medical Physics 36 (2009) 3192–204.

[25] S. Shannon, C. Agner, S. Soman, E. Libfeld, M. McDonald, K. Thomas, S. Englander, M. Rosen, D. Chin, J. Nosher, A. Madabhushi, Textural kinetics: a novel dynamic contrast-enhanced (DCE)-MRI feature for breast lesion classification, Journal of Digital Imaging 24 (2011) 446–463.

[26] J. Torrents-Barrena, D. Puig, M. Ferre, J. Melendez, L. Diez-Presa, M. Arenas, J. Marti, Breast masses identification through pixel-based texture classification, in: International Workshop on Digital Mammography, 2014, pp. 581–588.

[27] F. Honda, R. Nakayama, H. Koyama, A. Yamashita, Computer-aided diagnosis scheme for distinguishing between benign and malignant masses in breast DCE-MRI, Digital Imaging 29 (2016) 388–393.

[28] S. Lee, J. Kim, N. Cho, J. Park, Z. Yang, Y. Jung, K.M. Woo, Multilevel analysis of spatio temporal association features for differentiation of tumor enhancement patterns in breast DCE-MRI, Medical Physics 37 (2010) 56–3940.

[29] S. Francis, M. Sasikala, S. Saranya, Detection of breast abnormality from thermograms using curvelet transform based feature extraction, Journal of Medical Systems 23 (2014).

[30] B. Gupta, M. Tiwari, A tool supported approach for brightness preserving contrast enhancement and mass segmentation of mammogram images using histogram modified grey relational analysis, Multidimensional Systems and Signal Processing 28 (2017) 1549–1567.

[31] A. Vignati, V. Giannini, M. De Luca, L. Morra, D. Persano, L.A. Carbonaro, I. Bertotto, L. Martincich, D. Regge, A. Bert, Performance of a fully automatic lesion detection system for breast DCE-MRI, Journal of Magnetic Resonance Imaging 34 (2011) 1341–1351.

[32] S. Arora, J. Acharya, A. Verma, P.K. Panigrahi, Multilevel thresholding for image segmentation through a fast statistical recursive algorithm, Pattern Recognition Letters 29 (2008) 119–125.

[33] G. Kom, A. Tiedeu, M. Kom, Automated detection of masses in mammograms by local adaptive thresholding, Journal of Computers in Biology and Medicine 37 (2007) 37–48.

[34] S. Ribes, D.D. Laurent, N. Decoster, E. Gonneau, L. Risser, V. Feillel, O. Caselles, Automatic segmentation of breast mr images through a markov random field statistical model, IEEE Transactions on Medical Imaging 33 (2014) 1–11.

[35] V.K. Singh, S. Romani, H.A. Rashwan, F. Akram, N. Pandey, M. Sarker, Conditional generative adversarial and convolutional networks for x-ray breast mass segmentation and shape classification, in: Proceedings of the Medical Image Computing and Computer Assisted Intervention, 2018, pp. 833–840.

[36] R.K. Samala, L. Chan, H.-P. Hadjiiski, M.A. Helvie, C.D. Richter, K.H. Cha, Breast cancer diagnosis in digital breast tomosynthesis: Effects of training sample size on multi-stage transfer learning using deep neural nets, IEEE Transactions on Medical Imaging 38 (2019) 686–696.

[37] M. Saha, C. Chakraborty, Her2net: A deep framework for semantic segmentation and classification of cell membranes and nuclei in breast cancer evaluation, IEEE Transactions on Image Processing 27 (2018) 2189–2200.

[38] S.C. Agner, J. Xu, H. Fatakdawala, S. Ganesan, A. Madabhushi, S. Englander, J. Tomaszewski, Segmentation and classification of triple negative breast cancers using DCE-MRI, in: IEEE International Symposium on Biomedical Imaging: From Nano to Macro, IEEE, 2009, pp. 1227–1230.

[39] F. Aghaei, M. Tan, A.B. Hollingsworth, W. Qian, H. Liu, B. Zheng, Computer-aided breast MR image feature analysis for prediction of tumor response to chemotherapy, Medical Physics 42 (2015) 6520–6528.

[40] S.S. Reddi, S.F. Rudin, H.R. Keshavan, An optimal multiple threshold scheme for image segmentation, IEEE Transactions on Systems, Man, and Cybernetics 14 (1984) 661–665.

[41] A.H. Tuncay, I. Akduman, Realistic microwave breast models through T1-weighted 3-D MRI data, IEEE Transactions on Biomedical Engineering 62 (2015) 98–688.

[42] F. Retter, C. Plant, B. Burgeth, Computer-aided diagnosis for diagnostically challenging breast lesions in DCE-MRI based on image registration and integration of morphologic and dynamic characteristics, EURASIP Journal on Advances in Signal Processing 2013 (2013) 157.
[43] W. Lingle, B.J. Erickson, M.L. Zuley, R. Jarosz, E. Bonaccio, J. Filippini, G.N., Radiology data from the cancer genome atlas breast invasive carcinoma collection [tcga-brca], 2007.
[44] K. Clark, B. Vendt, K. Smith, J. Freymann, J. Kirby, P. Koppel, S. Moore, S. Phillips, D. Maffitt, M. Pringle, L. Tarbox, F. Prior, The cancer imaging archive (TCIA): Maintaining and operating a public information repository, 2013.
[45] G.M. ME, M.M. Subashini, Medical imaging with intelligent systems: A review, in: A.K. Sangaiah (Ed.), Deep Learning and Parallel Computing Environment for Bioengineering Systems, Academic Press, 2019, pp. 53–73. doi: 10.1016/B978-0-12-816718-2.00011-7.
[46] E.A. Hauth, C. Stockamp, S. Maderwald, A. Mühler, R. Kimmig, H. Jaeger, J. Barkhausen, M. Forsting, Evaluation of the three-time-point method for diagnosis of breast lesions in contrast-enhanced MR mammography, Clinic Imaging 30 (2006) 160–165.
[47] M.A. Balafar, A.R. Ramli, S. Mashohor, A new method for MR grayscale inhomogeneity correction, Artificial Intelligence Review 34 (2010) 195–204.
[48] D. Boukerroui, O. Basset, N. Guerin, A. Baskurt, Multiresolution texture based adaptive clustering algorithm for breast lesion segmentation, European Journal of Ultrasound 8 (1998) 135–144.
[49] C. Shannon, The mathematical theory of communication, The Bell System Technical Journal 27 (1948) 379–423.
[50] A. Tharwat, Classification assessment methods, Applied Computing and Informatics 17 (2018) 168–192.
[51] T. Si, A. De, A.K. Bhattacharjee, Segmentation of brain MRI using wavelet transform and grammatical bee colony, Journal of Circuits, Systems, and Computers 27 (2018) 1850108.
[52] F.J. Anscombe, The validity of comparative experiments, Journal of the Royal Statistical Society 111 (1948) 181–211.
[53] J.W. Tukey, Comparing individual means in the analysis of variance, Biometrics 5 (1949) 99–114.
[54] J. Derrac, S. Garcia, D. Molina, F. Herrera, A practical tutorial on the use of nonparametric statistical tests as a methodology for comparing evolutionary and swarm intelligence algorithms, Swarm and Evolutionary Computation 1 (2001) 3–18.
[55] G. Hommel, A stagewise rejective multiple test procedure based on a modified bonferroni test, Biometroka 75 (1988) 6–383.
[56] S. Brown, R. Tauler, B. Walczak, Comprehensive Chemometrics-Chemical and Biochemical Data Analysis, second ed., Elsevier, 2020.
[57] Y. Xue, B. Xue, M. Zhang, Self-adaptive particle swarm optimization for large-scale feature selection in classification, ACM Transactions on Knowledge Discovery from Data 13 (2019) 1–27.
[58] Y. Xue, Y. Tang, X. Xu, J. Liang, F. Neri, Multi-objective feature selection with missing data in classification, IEEE Transactions on Emerging Topics in Computational Intelligence (2021), https://doi.org/10.1109/TETCI.2021.3074147.